

CC Sculptoris: Eclipsing SU UMa-Type Intermediate Polar

Taichi KATO,^{1*} Franz-Josef HAMBSCH,^{2,3,4} Arto OKSANEN,⁵ Peter STARR,⁶ Arne HENDEN,⁷

¹ *Department of Astronomy, Kyoto University, Kyoto 606-8502*

**tkato@kustastro.kyoto-u.ac.jp*

² *Groupe Européen d’Observations Stellaires (GEOS), 23 Parc de Levesville, 28300 Bailleau l’Evêque, France*

³ *Bundesdeutsche Arbeitsgemeinschaft für Veränderliche Sterne (BAV), Munsterdamm 90, 12169 Berlin, Germany*

⁴ *Vereniging Voor Sterrenkunde (VVS), Oude Bleken 12, 2400 Mol, Belgium*

⁵ *Nyrola observatory, Jyvaskylan Sirius ry, Vertaalantie 419, FI-40270 Palokka, Finland*

⁶ *Warrumbungle Observatory, Tenby, 841 Timor Rd, Coonabarabran NSW 2357, Australia*

⁷ *American Association of Variable Star Observers, 49 Bay State Rd., Cambridge, MA 02138, USA*

(Received 201 0; accepted 201 0)

Abstract

We observed the 2014 superoutburst of the SU UMa-type intermediate polar CC Scl. We detected superhumps with a mean period of 0.05998(2) d during the superoutburst plateau and during three nights after the fading. During the post-superoutburst stage after three nights, a stable superhump period of 0.059523(6) d was detected. We found that this object is an eclipsing system with an orbital period of 0.058567233(8) d. By assuming that the disk radius in the post-superoutburst phase is similar to those in other SU UMa-type dwarf novae, we obtained a mass ratio of $q=0.072(3)$ from the dynamical precession rate of the accretion disk. The eclipse profile during outbursts can be modeled by an inclination of $80^{\circ}6\pm 0^{\circ}5$. The 2014 superoutburst was preceded by a precursor outburst and the overall appearance of the outburst was similar to superoutbursts in ordinary SU UMa-type dwarf novae. We showed that the standard thermal-tidal instability model can explain the outburst behavior in this system and suggest that inner truncation of the disk by magnetism of the white dwarf does not strongly affect the behavior in the outer part of the disk.

Key words: accretion, accretion disks — stars: novae, cataclysmic variables — stars: dwarf novae — stars: individual (CC Sculptoris)

1. Introduction

Cataclysmic variables (CVs) are close binary systems consisting of a white dwarf and a red (or brown) dwarf transferring the gas via Roche overflow [for a general review of CVs, see Warner (1995); Hellier (2001)]. Dwarf novae (DNe) are a subclass of CVs that show outbursts. SU UMa-type dwarf novae are a class of DNe that show long-lasting superoutbursts in addition to short, normal outbursts. During superoutbursts, superhumps, which have a period a few percent longer than the orbital period, are observed. It is widely believed that outbursts in DNe are caused by thermal instability of the accretion disk and superoutbursts and superhumps are caused by tidal instability arising from the 3:1 resonance in the accretion disk with the orbiting secondary [thermal-tidal instability (TTI) model; (Osaki 1989); see Osaki (1996) for a review]. Quite recently, this picture has become even more firmly established by analyses of Kepler observations (Osaki, Kato 2013a; Osaki, Kato 2013b).

Although the TTI model does not explicitly consider the effect of magnetism of the white dwarf, some CVs have magnetic fields of the white dwarf strong enough to affect the dynamics in the accretion disk. If the magnetic field is strong enough, the accretion disk cannot form and the transferred matter directly accretes on the magnetic

poles of the white dwarf. This condition is usually met in polars (AM Her-type objects) in which the strong magnetic field synchronizes the rotation of the white dwarf with the orbital period. In systems with weaker magnetic fields, disks can form but are truncated by the magnetic field in its inner part. This condition is usually met in intermediate polars (IPs) in which the white dwarf rotates asynchronously with the orbital period [for a review of IPs, see e.g. Patterson (1994)].

Several DNe have been confirmed to be IPs; especially notable are GK Per (Watson et al. 1985)¹ and DO Dra (Patterson et al. 1992; Patterson, Szkody 1993).² They are both objects above the period gap and are not expected to develop tidal instability. In recent years, several DNe below the period gap have been identified or proposed to be IPs, including CC Scl, the subject of this paper. The inner disk is supposed to be truncated in such systems, and it may affect the global dynamics of the disk in outburst. Such a system is expected to provide us insight into the effect of magnetism in development of outbursts and superoutbursts, and may eventually help us better understanding the mechanism of outbursts and superhumps.

¹ Although GK Per is usually considered as a classical nova, it also shows dwarf nova-type outbursts (e.g. Bianchini et al. 1986).

² Also referred to as YY Dra.

2. CC Sculptoris

CC Scl was discovered as a ROSAT source (RX J2315.5–3049) and was optically identified as a dwarf nova, although outbursts had not been detected (Schwope et al. 2000). R. Stubbings visually detected two outbursts in 2000 (vsnet-outburst 245, 810). During the second outburst, Ishioka et al. (2001) detected likely superhumps with a period of 0.078 d and amplitudes of ~ 0.3 mag. The orbital period, however, was reported to be much shorter (0.058 d) according to Augusteijn et al. (2000, vsnet-campaign 544). Ishioka et al. (2001) interpreted that this discrepancy may be understood if the object is an IP. The shorter period was later confirmed to be the orbital period (Chen et al. 2001; Tappert et al. 2004).

During the 2011 superoutburst, Kato et al. (2013a) detected superhumps with a mean period of 0.0600 d. Kato et al. (2013a), using the least absolute shrinkage and selection operator (Lasso) method (Tibshirani 1996; Kato, Uemura 2012), demonstrated that the irregular profiles seen in the superhumps in this systems are caused by the superposition of superhumps and orbital modulations. Woudt et al. (2012), partly using the same data as in Kato et al. (2013a), identified a superhump period of 1.443 hr (0.0601 d) and also showed that the object is an IP with a spin period of 0.00450801(6) d (389.49 s).

There was an outburst in 2012 August, which turned out to be a normal outburst (vsnet-alert 14880, 14892).³ There was also a normal outburst in 2013 January (vsnet-alert 15307).

3. Observations and Analysis

The 2014 superoutburst was detected by P. Starr on July 2 (cvnet-outburst 6019). The initial peak was actually a precursor outburst and the main superoutburst followed five days later (vsnet-alert 17483). Time-series observations during this outburst started relatively late and were rather sparse compared to the 2011 observation. Although superhumps were detected, the object started fading rapidly within three days (vsnet-alert 17491). We only observed the later part of the superoutburst.

The summary of observations, with mean magnitudes, are listed in table 1. The observer’s codes are P. Starr (SPE, 50cm telescope, Warrumbungle Observatory), F.-J. Hambsch (HMB, 40cm telescope in San Pedro de Atacama, Chile) and A. Oksanen (OAR, Harlinton Observatory 50cm Planewave telescope in San Pedro de Atacama, Chile).

In period analysis, we used the 2011 observation (Kato et al. 2013a) and the 2012 and 2013 observations from the public data in the AAVSO database⁴ in addition to the 2014 observations. We also used the Catalina Real-time Transient Survey (CRTS; Drake et al. 2009)⁵ for determining the orbital period.

We adjusted the zero-points between observers and all observations were converted to Barycentric Julian Days (BJD). In making period analysis or obtaining phase-averaged light curves, we removed the long-term trends by using locally-weighted polynomial regression (LOWESS; Cleveland 1979).

We used phase dispersion minimization (PDM; Stellingwerf 1978) for period analysis and 1σ errors for the PDM analysis was estimated by the methods of Fernie (1989) and Kato et al. (2010). We analyzed 100 samples which randomly contain 50% of observations, and performed PDM analysis for these samples. The bootstrap result is shown as a form of 90% confidence intervals in the resultant θ statistics.

4. Results

4.1. Overall Light Curve of Outburst

The overall light curve (lower panel of figure 1) clearly indicates the presence of a precursor outburst, followed by temporary fading for at least two days. Although the start of the main superoutburst was not covered by observations, its duration was less than 9 d. This duration is shorter than typical ones (10–14 d) in SU UMa-type dwarf novae with short orbital periods (e.g. Nogami et al. 1998; Baba et al. 2000). There was no post-superoutburst rebrightening.

The mean fading rate from the precursor outburst for the first two days was 0.84(3) mag d⁻¹, which is somewhat slower than fading rates of normal outbursts in SU UMa-type dwarf novae. The mean fading rate of the plateau stage of the superoutburst was 0.11(1) mag d⁻¹, which is also typical for an SU UMa-type dwarf nova other than candidate period bouncers (Kato et al. 2014b). The mean fading rate during the rapid fading from the plateau phase was 1.69(2) mag d⁻¹. Slow fading at a rate of 0.021(1) mag d⁻¹ continued for more than 20 d after the rapid fading. This feature is frequently seen in SU UMa-type dwarf novae with infrequent outbursts or in WZ Sge-type dwarf novae.

4.2. Superhumps during Superoutburst and Early Post-Superoutburst

The times of superhump maxima were determined by the template fitting method as described in Kato et al. (2009a). The results during the superoutburst are listed in table 2. Due to the limited coverage during the superoutburst, the statistics were rather poor. As shown later (subsection 5.1), this superhump period persisted up to three days after the rapid fading from the superoutburst plateau. Figure 2 shows the PDM analysis and phase-averaged profile during the superoutburst and the three nights just after the superoutburst. The best period by the PDM method was 0.05998(2) d.

4.3. Post-Superoutburst Superhumps

During the post-superoutburst stage except the initial three nights, a PDM analysis yielded a stable period of 0.059523(6) d (figure 3). The period is considerably

³ VSNET archive can be accessed at (for example, alert messages) <<http://ooruri.kusastro.kyoto-u.ac.jp/pipermail/vsnet-alert/>>.

⁴ <<http://www.aavso.org/data-download>>.

⁵ <<http://nessi.cacr.caltech.edu/catalina/>>.

Table 1. Log of observations.

Start*	End*	Mean Mag.	Error	N^\dagger	Observer	Filter [‡]
56841.2786	56841.2833	15.089	0.028	5	SPE	CV
56842.2787	56842.2834	15.929	0.022	5	SPE	CV
56843.2777	56843.2823	16.281	0.039	5	SPE	CV
56846.2485	56846.2658	13.604	0.037	8	SPE	CV
56847.1636	56847.1778	13.512	0.023	10	SPE	CV
56848.3128	56848.3212	13.886	0.017	6	SPE	CV
56849.1717	56849.2915	14.135	0.009	195	SPE	CV
56850.0837	56850.1978	14.129	0.010	174	SPE	V
56851.7989	56851.9274	14.454	0.032	39	HMB	CV
56852.1178	56852.2399	15.229	0.019	66	SPE	V
56852.7910	56852.9166	16.477	0.007	296	OAR	CV
56852.7959	56852.9276	16.349	0.027	39	HMB	CV
56853.6983	56853.9167	16.415	0.007	286	OAR	CV
56853.7932	56853.9282	16.439	0.023	43	HMB	CV
56854.7914	56854.9279	16.526	0.018	52	HMB	CV
56854.8147	56854.9167	16.729	0.009	131	OAR	CV
56855.7348	56855.9164	16.573	0.011	236	OAR	CV
56855.7885	56855.9254	16.641	0.018	52	HMB	CV
56856.7999	56856.9169	16.671	0.011	151	OAR	CV
56856.8046	56856.9263	16.675	0.024	39	HMB	CV
56857.7322	56857.9164	16.631	0.007	240	OAR	CV
56857.7851	56857.9256	16.621	0.017	57	HMB	CV
56858.7823	56858.9328	16.703	0.016	61	HMB	CV
56859.2866	56859.2955	16.749	0.063	10	SPE	V
56859.7795	56859.9320	16.607	0.021	62	HMB	CV
56860.2678	56860.2766	16.584	0.049	10	SPE	V
56860.7767	56860.9318	16.647	0.018	63	HMB	CV
56861.2658	56861.2668	16.557	0.035	2	SPE	CV
56861.7739	56861.8067	16.745	0.048	10	HMB	CV
56862.7711	56862.9317	16.748	0.017	65	HMB	CV
56863.7685	56863.9310	16.483	0.024	66	HMB	CV
56864.7657	56864.9315	16.874	0.014	56	HMB	CV

*BJD–2400000.

†Number of observations.

‡CV indicates unfiltered observations.

Table 2. Superhump maxima of CC Scl (2014)

E	max*	error	$O - C^\dagger$	phase [‡]	N^\S
0	56849.2357	0.0014	0.0076	0.38	81
15	56850.1246	0.0015	–0.0014	0.56	79
16	56850.1774	0.0011	–0.0085	0.46	64
44	56851.8594	0.0021	–0.0025	0.18	15
60	56852.8348	0.0011	0.0151	0.83	126
62	56852.9290	0.0052	–0.0104	0.44	51

*BJD–2400000.

†Against max = 2456849.2281 + 0.059859 E .

‡Orbital phase.

§Number of points used to determine the maximum.

shorter than the period of superhumps during the super-outburst. The times of post-superoutburst maxima (including the initial three nights) are listed in table 3.

4.4. Orbital Variations

The reported orbital period of 0.05763 d (Woudt et al. 2012) could not be detected in the analysis of the post-superoutburst data (figure 3). We should note that if 0.05763 d is the true orbital period, the fractional superhump excess $\epsilon \equiv P_{\text{SH}}/P_{\text{orb}} - 1 = 4.3\%$, using the values in Woudt et al. (2012), is too large for this orbital period.

We alternately propose the orbital period of 0.058566(2) d detected in the PDM analysis of the post-superoutburst observations (figure 3). This value is in good agreement with the one 0.05845 d by Chen et al. (2001) and the period [0.0585845(10) d] detected during the 2011 observation (Kato et al. 2013a). By adopting this period, the orbital light curve turned out

Table 1. Log of observations (continued).

Start*	End*	Mean Mag.	Error	N^\dagger	Observer	Filter ‡
56865.0475	56865.0485	16.603	0.157	2	SPE	CV
56865.7629	56865.9315	16.932	0.015	57	HMB	CV
56866.0201	56866.0211	16.897	0.052	2	SPE	CV
56866.7601	56866.9296	16.887	0.018	58	HMB	CV
56867.0184	56867.0194	16.911	0.014	2	SPE	CV
56867.7575	56867.9291	16.769	0.018	58	HMB	CV
56868.1102	56868.1111	16.483	0.150	2	SPE	CV
56868.7545	56868.9282	16.881	0.013	60	HMB	CV
56869.1737	56869.1747	16.699	0.120	2	SPE	CV
56869.7518	56869.9291	16.923	0.017	60	HMB	CV
56869.8215	56869.9163	16.897	0.011	126	OAR	CV
56870.0318	56870.0327	16.834	0.063	2	SPE	CV
56870.7490	56870.9291	16.912	0.017	61	HMB	CV
56871.1968	56871.1978	16.995	0.051	2	SPE	CV
56871.7462	56871.9293	16.923	0.017	62	HMB	CV
56871.7568	56871.9168	16.903	0.007	208	OAR	CV
56872.0608	56872.0618	16.598	0.039	2	SPE	CV
56872.7434	56872.9258	16.981	0.015	62	HMB	CV
56873.0342	56873.0352	16.754	0.129	2	SPE	CV
56873.7406	56873.9282	16.924	0.015	64	HMB	CV
56874.0589	56874.0589	16.288	–	1	SPE	CV
56874.7386	56874.9258	16.976	0.017	63	HMB	CV
56875.0108	56875.0118	16.664	0.048	2	SPE	CV
56875.7358	56875.9263	16.995	0.015	64	HMB	CV
56875.9991	56876.0001	16.700	0.042	2	SPE	CV
56876.7330	56876.9288	16.939	0.016	66	HMB	CV
56877.0326	56877.0336	17.038	0.233	2	SPE	CV
56878.0904	56878.0914	17.101	0.201	2	SPE	CV
56879.1822	56879.1832	16.848	0.042	2	SPE	CV
56879.7247	56879.9118	16.991	0.024	60	HMB	CV
56880.7218	56880.9111	17.071	0.034	64	HMB	CV
56881.0641	56881.0651	16.940	0.046	2	SPE	CV
56882.9707	56882.9717	17.049	0.045	2	SPE	CV

*BJD–2400000.

 † Number of observations. ‡ CV indicates unfiltered observations.

to show a shallow eclipse with double orbital humps.⁶ Figure 4 represents quiescent time-series observations for 2011–2014 when the magnitude was fainter than 16 (these observations include post-superoutburst observations). It is worth noting that Chen et al. (2001) correctly referred to a dip observed in the light curve as a possible eclipse. The ephemeris of eclipses using all the available data (2011, 2012, 2014 outburst and post-outburst observations) and the CRTS data was determined by Markov-chain Monte Carlo (MCMC) method, which was introduced in Kato et al. (2013a), as follows:

$$\text{Min(BJD)} = 2456668.00638(9) + 0.058567233(8)E. \quad (1)$$

Since the times of individual eclipses are difficult to determine, we instead give the mean epoch [BJD 2456863.5624(1)] of the eclipse observations after the 2014

superoutburst. The phase plot of the CRTS observations is also shown in figure 5. Although eclipses are not very clear in the CRTS data, orbital modulations having a hump maximum around phase 0.8 were recorded and the overall appearance appears to be consistent with the 2014 post-superoutburst observations in quiescence.

The quiescent orbital profile resembles those of low mass-transfer rate objects such as WZ Sge-type dwarf novae [see e.g. WZ Sge and AL Com (Patterson et al. 1996), V455 And (Araujo-Betancor et al. 2005; Kato et al. 2009a), V386 Ser (Mukadam et al. 2010), EZ Lyn (Kato et al. 2009b; Zharikov et al. 2013), BW Scl (Augusteijn, Wisotzki 1997; Kato et al. 2013a)], although the double-wave orbital humps are less clear in CC Scl. A classical interpretation assuming a semi-transparent accretion disk allowing the light from the hot spot to escape in two directions (Skidmore et al. 2000) would be a viable interpretation.

⁶ A. Oksanen also noticed the presence of eclipse-like fading during the 2013 observations in quiescence.

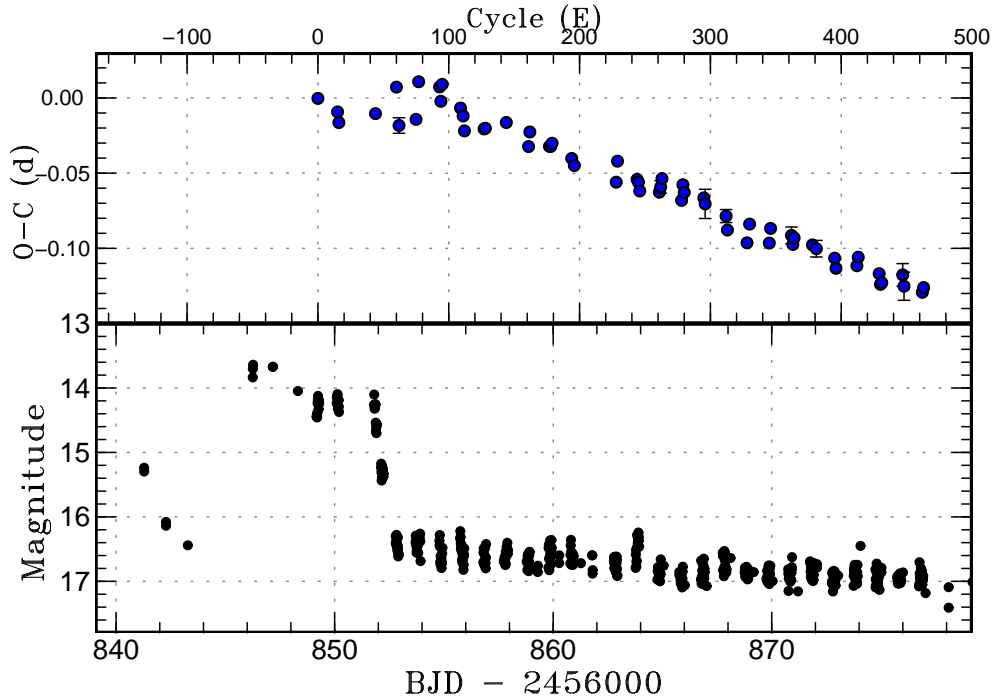


Fig. 1. $O-C$ diagram of superhumps in CC Scl (2014). (Upper): $O-C$ diagram. A period of 0.05986 d was used to draw this figure. A longer superhump period (stage B) was observed during the superoutburst. After fading from the superoutburst plateau, there was a transition to a shorter constant period (stage C superhumps). There was no phase jump between them. (Lower): Light curve. The observations were binned to 0.01 d. A precursor outburst was clearly detected.

Although eclipses became less apparent in outburst, they continued to be present (figure 6). Orbital humps almost disappeared in outburst.

5. Discussion

5.1. Identification of Superhump Stages

By using the new orbital period, the fractional superhumps excesses are found to be within a reasonable region: 2.6% for the 2011 data, 2.4% for the 2014 data during superoutburst and 1.6% for the post-superoutburst data in 2014, respectively.

In most SU UMa-type dwarf novae, shortening of the superhump period is not usually observed following the rapid fading from the superoutburst, and the period after the fading is usually the same as that of stage C superhumps, which are late-stage superhumps with almost constant periods [for the definition of superhump stages, see Kato et al. (2009a)]. Such shortening of the superhump period immediately following the rapid decline apparently is unique to CC Scl.

The difference of fractional superhump excesses during the superoutburst and post-superoutburst is 0.8–1.0%, which is similar to what is usually observed between stage B and C superhumps (Kato et al. 2009a). We therefore identify the superhumps during the post-superoutburst phase to be stage C superhumps and those during the superoutburst to be stage B superhumps, respectively. There was no phase jump between these stages (see upper panel of figure 1). There was no evidence of “traditional”

late superhumps, in which an ~ 0.5 phase jump is observed (e.g. Vogt 1983). This finding strengthens our interpretation of the period change as stage B–C transition [see Kato et al. (2009a) for the lack of a phase jump between stages B and C].

Since the duration of the 2014 superoutburst was relatively short (less than 9 d excluding the precursor part; the duration of the 2011 superoutburst was less constrained but was shorter than 11 d), it may be possible that the superoutburst ended earlier than in other SU UMa-type dwarf novae and the stage B–C transition was consequently recorded in the later phase of the outburst than in other SU UMa-type dwarf novae. Such early termination of the outburst can be reasonably explained assuming that the inner part of the disk is drained by the magnetic field of the white dwarf (Woudt et al. 2012). Since stage B–C transition was not apparently affected by this effect, we can suggest that stage C superhumps originate from the outer part of the accretion disk, rather than the inner part. Further observations of superhumps in such systems may shed light on the origin of still unresolved stage C superhumps.

5.2. Orbital Parameters

Since we did not observe stage A superhumps, we could not directly apply the modern method of estimating the mass ratio (q) from the fractional superhump excess (Kato, Osaki 2013). We can, however, constrain q using the post-superoutburst superhumps. This method was introduced in Kato et al. (2013b). We repeat the essence of

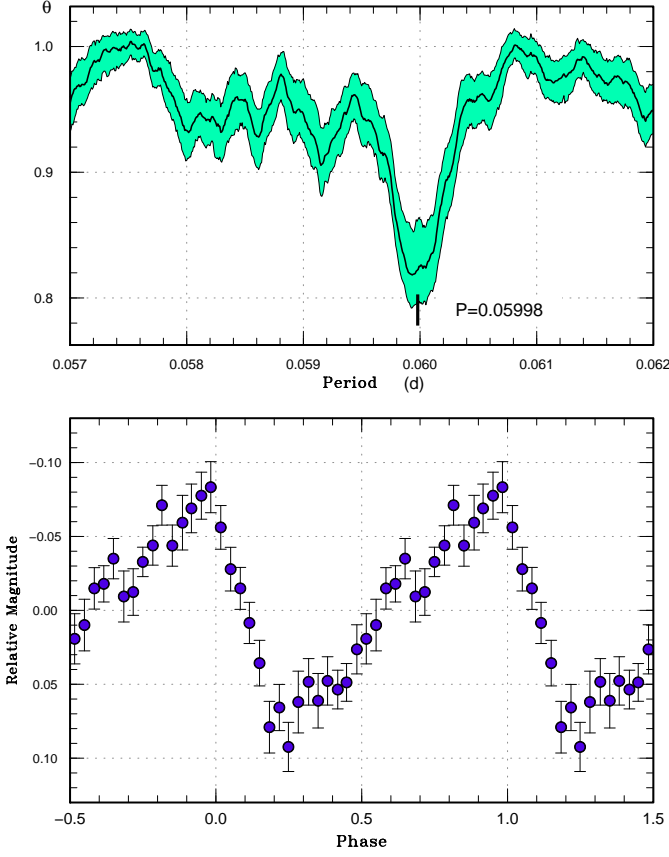


Fig. 2. Superhumps in CC Scl during superoutburst and three nights just after the superoutburst (2014). (Upper): PDM analysis. The 90% confidence intervals by the bootstrapping method (see text for the details) is shown by two curves above and below the central curve. (Lower): Phase-averaged profile by the superhump period of 0.05998 d.

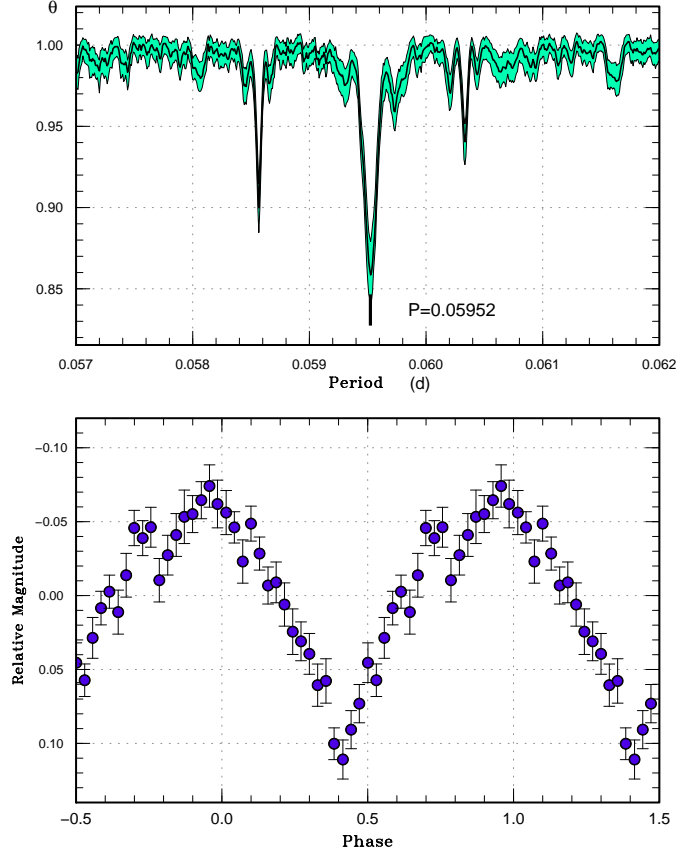


Fig. 3. Superhumps in CC Scl in the postsuperoutburst phase (2014). (Upper): PDM analysis. The sharp signal at 0.05857 d is the orbital period. The 90% confidence intervals by the bootstrapping method (see text for the details) is shown by two curves above and below the central curve. (Lower): Phase-averaged profile by the superhump period of 0.059523 d.

the method for clarity.

The dynamical precession rate, ω_{dyn} in the disk can be expressed by (see, Hirose, Osaki 1990):

$$\omega_{\text{dyn}}/\omega_{\text{orb}} = Q(q)R(r), \quad (2)$$

where ω_{orb} and r are the angular orbital frequency and the dimensionless radius measured in units of the binary separation A . The dependence on q and r are

$$Q(q) = \frac{1}{2} \frac{q}{\sqrt{1+q}}, \quad (3)$$

and

$$R(r) = \frac{1}{2} \frac{1}{\sqrt{r}} b_{3/2}^{(1)}(r), \quad (4)$$

where $\frac{1}{2}b_{s/2}^{(j)}$ is the Laplace coefficient

$$\frac{1}{2}b_{s/2}^{(j)}(r) = \frac{1}{2\pi} \int_0^{2\pi} \frac{\cos(j\phi)d\phi}{(1+r^2-2r\cos\phi)^{s/2}}, \quad (5)$$

This $\omega_{\text{dyn}}/\omega_{\text{orb}}$ is equivalent to the fractional superhump excess (in frequency) $\epsilon^* \equiv 1 - P_{\text{orb}}/P_{\text{SH}}$ and it is related

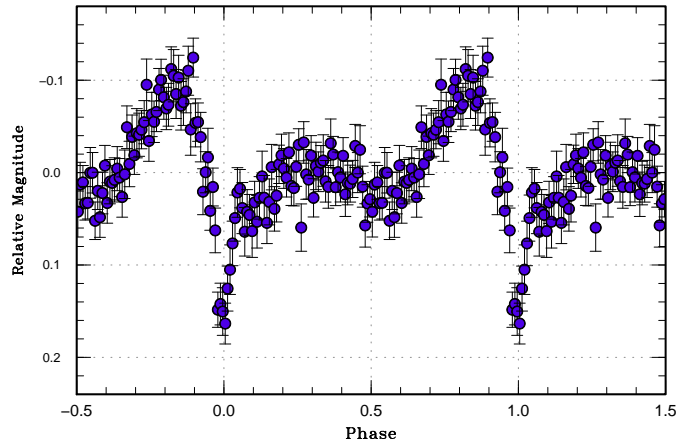


Fig. 4. Mean orbital light curve of CC Scl in quiescence. The ephemeris of equation (1) is used. Time-series observations fainter than 16 mag were used.

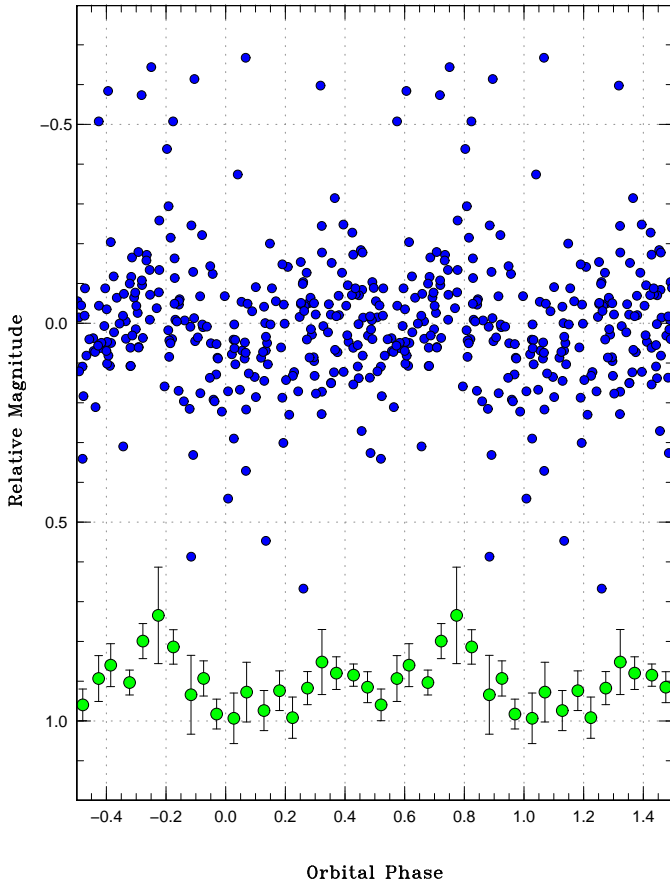


Fig. 5. Orbital light curve of CC Scl from the CRTS data in quiescence. The ephemeris of equation (1) is used. Long-term trends were subtracted. Typical errors of the CRTS observations were 0.10–0.18 mag. In the lower part of the figure, phase-averaged data to 20 bins are plotted with larger symbols and 1σ errors.

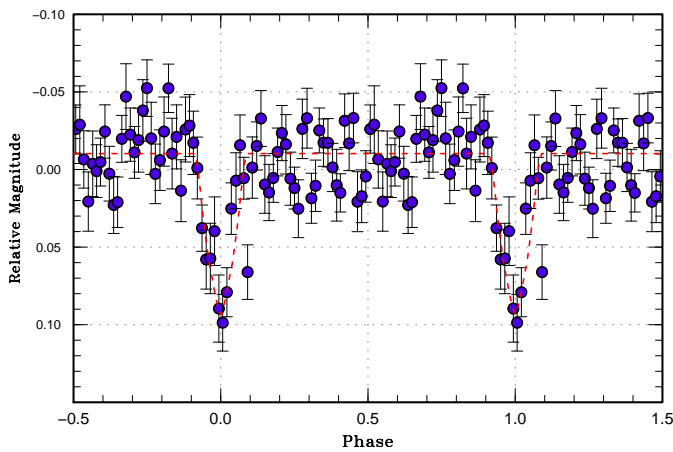


Fig. 6. Mean orbital light curve of CC Scl in outburst. The ephemeris of equation (1) is used. Time-series observations during the 2011, 2012 and 2014 outbursts were used. The dashed line represents a model with $q=0.072$, $i=80^\circ.6$ and disk radius of 0.41A (see subsection 5.2).

Table 3. Superhump maxima of CC Scl (2014) (post-superoutburst)

E	max [*]	error	$O - C^\dagger$	phase [‡]	N^\S
0	56853.7113	0.0033	-0.0174	0.80	45
2	56853.8560	0.0022	0.0084	0.27	75
18	56854.8103	0.0009	0.0104	0.56	38
19	56854.8606	0.0024	0.0012	0.42	75
20	56854.9318	0.0021	0.0128	0.64	36
34	56855.7540	0.0009	0.0019	0.68	51
36	56855.8685	0.0009	-0.0027	0.63	78
37	56855.9184	0.0019	-0.0123	0.48	36
52	56856.8176	0.0008	-0.0058	0.84	54
53	56856.8779	0.0007	-0.0050	0.87	79
69	56857.8395	0.0010	0.0043	0.29	82
86	56858.8412	0.0013	-0.0058	0.39	22
87	56858.9107	0.0024	0.0043	0.58	20
102	56859.7990	0.0012	-0.0002	0.74	13
103	56859.8589	0.0015	0.0002	0.76	20
104	56859.9208	0.0015	0.0026	0.82	17
119	56860.8086	0.0018	-0.0024	0.98	17
121	56860.9236	0.0032	-0.0063	0.95	16
153	56862.8281	0.0018	-0.0064	0.46	21
154	56862.9019	0.0023	0.0079	0.72	20
169	56863.7877	0.0016	0.0010	0.85	12
170	56863.8457	0.0014	-0.0006	0.84	21
171	56863.8997	0.0022	-0.0060	0.76	20
186	56864.7968	0.0031	-0.0017	0.08	14
187	56864.8601	0.0041	0.0021	0.16	16
188	56864.9256	0.0025	0.0081	0.28	12
203	56865.8090	0.0022	-0.0013	0.36	17
204	56865.8792	0.0017	0.0095	0.56	16
205	56865.9340	0.0031	0.0047	0.49	9
220	56866.8283	0.0018	0.0062	0.76	17
221	56866.8841	0.0097	0.0026	0.72	17
237	56867.8338	0.0043	0.0000	0.93	16

^{*}BJD-2400000.

[†]Against max = 2456853.7286 + 0.059515E.

[‡]Orbital phase.

[§]Number of points used to determine the maximum.

to the conventional fractional superhump excess (in period) ϵ by a relation $\epsilon^* = \epsilon/(1 + \epsilon)$. This dynamical precession rate is considered to be equal to the observed ϵ^* when the pressure effect can be ignored. This condition is achieved either if the superhumps are confined to the region of the 3:1 resonance (stage A superhumps) or the disk is cold such as in a state of post-superoutburst superhumps (Osaki, Kato 2013b).

We can express fractional superhump excesses (in frequency unit) of post-superoutburst superhumps as follows:

$$\epsilon^*(\text{post}) = Q(q)R(r_{\text{post}}), \quad (6)$$

where $\epsilon^*(\text{post})$ and r_{post} are the fractional superhump excess and disk radius immediately after the outburst, respectively.

In various SU UMa-type objects other than WZ Sge-

Table 3. Superhump maxima of CC Scl (2014) (post-superoutburst, continued)

E	max*	error	$O - C^\dagger$	phase‡	N^\S
238	56867.8844	0.0037	-0.0089	0.80	16
253	56868.7738	0.0014	-0.0123	0.98	11
255	56868.9059	0.0027	0.0008	0.24	16
270	56869.7912	0.0036	-0.0066	0.35	16
271	56869.8608	0.0015	0.0035	0.54	78
287	56870.8139	0.0056	0.0044	0.82	17
288	56870.8678	0.0023	-0.0013	0.73	16
289	56870.9320	0.0037	0.0034	0.83	9
303	56871.7654	0.0012	0.0036	0.06	47
306	56871.9424	0.0055	0.0021	0.08	12
320	56872.7742	0.0016	0.0006	0.29	14
321	56872.8273	0.0019	-0.0058	0.19	16
337	56873.7867	0.0029	0.0014	0.57	17
338	56873.8523	0.0038	0.0075	0.69	16
354	56874.7991	0.0024	0.0020	0.86	17
355	56874.8519	0.0024	-0.0047	0.76	16
356	56874.9128	0.0029	-0.0034	0.80	15
372	56875.8758	0.0075	0.0074	0.24	17
373	56875.9281	0.0094	0.0002	0.14	10
387	56876.7621	0.0027	0.0010	0.38	13
388	56876.8251	0.0022	0.0045	0.45	16
438	56879.7918	0.0050	-0.0046	0.11	16
454	56880.7411	0.0041	-0.0075	0.32	11
455	56880.8066	0.0055	-0.0015	0.44	16

*BJD-2400000.

†Against max = 2456853.7286 + 0.059515E.

‡Orbital phase.

§Number of points used to determine the maximum.

type dwarf novae with multiple rebrightenings, the value of r_{post} has been experimentally known to be in a narrow region 0.37–0.38 A , where A is the binary separation (Kato, Osaki 2013). By assuming this r_{post} in CC Scl, we can estimate $q=0.072(3)$ (the error corresponds to the error of ϵ^*). This value is within a range of $0.06 < q < 0.09$ in Chen et al. (2001), who assumed the mass-radius relation for a normal lower main-sequence secondary.

By assuming $q=0.072$, we can constrain the binary inclination by modeling the eclipse profile in outburst. As in the section of MASTER OT J005740.99+443101.5 in Kato et al. (2014a), we modeled the eclipse light curve. We assumed flat and axisymmetric geometry and a standard disk having a surface luminosity with a radial dependence $\propto r^{-3/4}$ (i.e. assuming that we observed the Rayleigh-Jeans tail of the emission from the hot disk). The secondary is assumed to fill the Roche lobe. Although these assumptions on the disk are rough, they will not seriously affect the results. In the present case, this is because the central part of this disk needs to be grazingly eclipsed to reproduce the shallow eclipse in outburst, and the result is very insensitive to the condition in the outer part of the disk (either radius or the existence of disk flaring). For an optically thick disk with a broad range of radius 0.33–0.46 A , an inclination value of $i=80.6^\circ$ best reproduced the

observed eclipse depth of 0.11 mag (figure 6, in which the case of 0.41 A is shown as an example). The uncertainty in i was less than 0.5° .

The depth of eclipses is deeper in quiescence. This is likely caused by the contribution from the hot spot.

5.3. Spin Modulations

After the detection of the IP spin modulations by Woudt et al. (2012), we re-examined our data in 2011 and examined the present data in 2014. The spin period could be detected in outburst observations both in 2011 and 2014. Using the PDM method, the 2011 observation yielded a period of 0.0045076(2) d (amplitude 0.09 mag) and the 2014 one yielded 0.0045079(9) d (amplitude 0.08 mag). Post-outburst data yielded weaker signals: 0.06 mag in 2011 and 0.04 mag in 2014 in amplitude. Examples of Lasso 2-D power spectrum analysis (cf. Kato, Maehara 2013) are shown in figures 7 (the 2011 superoutburst) and 8 (the 2014 superoutburst). Spin modulations in post-superoutburst stage were not clearly detected in Lasso analysis since short (2.5 d) windows were used. Since the system brightness faded by ~ 3 mag after the superoutburst, the pulsed flux decreased by a factor of 15–30 after the outburst. This phenomenon can be naturally understood by considering that the pulsed flux reflects the intensity of the accretion column on the magnetic pole and that the accretion rate dramatically decreased after the outburst. This behavior is consistent with X-ray observations in Woudt et al. (2012).

5.4. Implication on Disk Instability Model

Among IPs, V455 And (Araujo-Betancor et al. 2005; Silvestri et al. 2012) has been the only object that showed a WZ Sge-type superoutburst [although there has been a claim that WZ Sge (e.g. Warner, Pretorius 2008) is also an IP, the situation is less clear]. CC Scl is the first IP that confidently exhibits a superoutburst of an ordinary SU UMa-type dwarf nova, rather than an extreme superoutburst of a WZ Sge-type dwarf nova. This finding suggests that the basic mechanism causing ordinary SU UMa-type superoutbursts is not strongly affected by the magnetism of the white dwarf. The standard TTI model (Osaki 1989) requires the 3:1 resonance to trigger a superoutburst. The radius of the 3:1 resonance is the outermost achievable radius in ordinary SU UMa-type dwarf novae. This radius is larger than any radius in outburst cycles of normal outbursts, and if the disk is sufficiently present (or not so strongly truncated) to exhibit normal outbursts, we can expect that the magnetism will less affect the disk at the radius of the 3:1 resonance. We can thus expect to see superoutbursts if the total angular momentum accumulates during the cycles of normal outbursts and the disk radius eventually reaches the 3:1 resonance on the occasion of an outburst. This is exactly what is seen in CC Scl, and the observed behavior is in agreement with the TTI model considering a partial truncation of the inner disk.

It is worth noting that a precursor outburst was also seen in CC Scl. In the TTI model, the precursor outburst

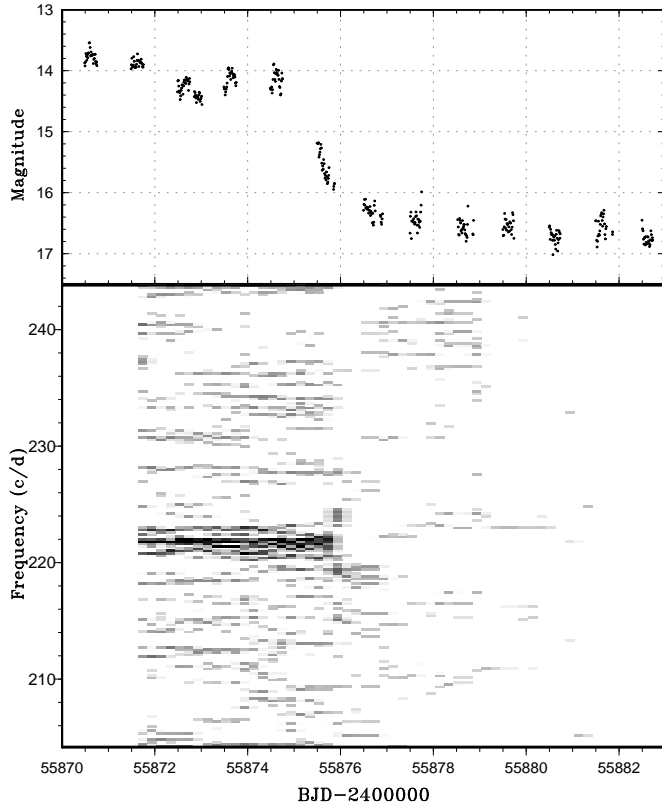


Fig. 7. Lasso 2-D power spectrum analysis of the spin period in CC Scl (2011). (Upper): Light curve. The data were binned to 0.01 d. (Lower): Result of the lasso analysis ($\log \lambda = -8.5$). The frequency 221.8 c/d corresponds to the spin period. The spin modulations became strongest around the end of the superoutburst, and then decayed quickly. The width of the sliding window and the time step used are 2.5 d and 0.2 d, respectively.

is the final normal outburst during which the expansion of the disk brings its radius to the 3:1 resonance. Since this phenomenon takes place also in the outermost part of the disk, it would be a natural consequence that magnetism does not strongly affect the appearance of the precursor outburst.

We should discuss the outburst behavior of other IPs among dwarf novae below the period gap. HT Cam is an established IP (Tovmassian et al. 1998; Kemp et al. 2002; Evans, Hellier 2005; de Martino et al. 2005). This object shows only brief outbursts with extremely rapid fading rates (Kemp et al. 2002; Ishioka et al. 2002). These outbursts are reported to occur quasi-cyclically, and can be regarded as a consequence of thermal instability (Ishioka et al. 2002; Woudt et al. 2012). Despite that HT Cam should have a mass ratio low enough to develop the 3:1 resonance, no superoutburst has been recorded. As discussed in Woudt et al. (2012), the disk in HT Cam may be more strongly truncated than in CC Scl, and this may be responsible for the difference in outburst behavior. We should continue to see whether HT Cam never shows a superoutburst.

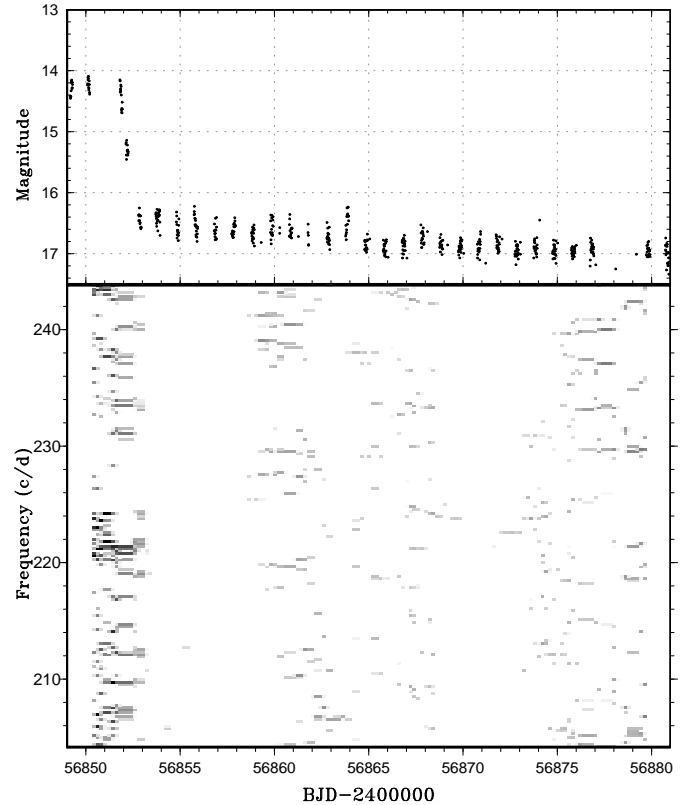


Fig. 8. Lasso 2-D power spectrum analysis of the spin period in CC Scl (2014). (Upper): Light curve. The data were binned to 0.01 d. (Lower): Result of the lasso analysis ($\log \lambda = -8.5$). The frequency 221.8 c/d corresponds to the spin period. The spin modulations were detected during the superoutburst but were not clearly detected after the ending of the superoutburst. Note that the observation statistics was better in 2011. The width of the sliding window and the time step used are 2.5 d and 0.2 d, respectively.

FS Aur is an enigmatic object below the period gap. Although this object has an orbital period of 0.05958096(5) d (Thorstensen et al. 1996; Neustroev et al. 2013), only short (normal) outbursts were observed with short (~ 12 d) recurrence times (Geßner 1989; Andronov 1991). Neustroev et al. (2012) reported that the recurrence time of the normal outbursts was relatively short and stable (18 ± 2.5 d). VSNET and AAVSO observations since 2010 have basically confirmed this outburst property. Neustroev et al. (2013) suggested that this object is an IP. The light behavior, however, is totally different from either HT Cam or CC Scl. FS Aur shows short outbursts similar to ordinary SU UMa-type normal outbursts, and does not show extremely rapid fading as seen in HT Cam [the fading rate during the linear fading part is reported to be ~ 0.8 mag d^{-1} (Neustroev et al. 2012), which is an ordinary value for normal outbursts of SU UMa-type dwarf novae.⁷] Judging only from the morphology of

⁷ Although faster (~ 2 mag d^{-1}) fading rate was reported in the final stage of outbursts (Neustroev et al. 2012), our examination suggests that this feature is not present in many of outbursts

outbursts, there does not seem to be an indication of truncation of the disk. Some outbursts of FS Aur are longer than others, but superhumps have not yet been definitely detected. Both the IP status of this object and the possible presence of a superoutburst or superhumps need to be explored further.

6. Summary

We observed the 2014 superoutburst of the SU UMa-type intermediate polar CC Scl. We detected superhumps with a mean period of 0.05998(2) d during the superoutburst plateau and during three nights after the fading. During the post-superoutburst stage after three nights, a stable period of 0.059523(6) d was detected. In addition to these periods, we found that this object has shallow eclipses and reached the identification of the orbital period of 0.058567233(8) d by using the available data since 2011 and the CRTS data in quiescence. We identified the superhump period during the superoutburst plateau to be stage B superhumps (according to the definition by Kato et al. 2009a) and post-superoutburst superhumps to be stage C superhumps. Such a late transition to stage C superhumps has not been observed in other systems and we consider that premature quenching of the superoutburst may be responsible for this phenomenon. By adopting the experimentally determined disk radii in other SU UMa-type dwarf novae in the post-superoutburst phase, we obtained a mass ratio of $q=0.072(3)$ from the dynamical precession rate of the accretion disk. A modeling of the eclipse profile during outbursts yielded an inclination of $80.6 \pm 0.5^\circ$. The 2014 superoutburst was preceded by a precursor outburst and the overall appearance of the outburst was similar to a superoutburst in ordinary SU UMa-type dwarf novae. We discuss that the standard thermal-tidal instability model can explain the outburst behavior in this system and suggest that inner truncation of the disk by magnetism of the white dwarf does not strongly affect the behavior in the outer part of the disk. Spin modulations were also recorded during outbursts, and were enhanced by a factor of 15–30 compared to the post-superoutburst state. This can be naturally explained by the increased accretion rate during outbursts.

This work was supported by the Grant-in-Aid “Initiative for High-Dimensional Data-Driven Science through Deepening of Sparse Modeling” from the Ministry of Education, Culture, Sports, Science and Technology (MEXT) of Japan. We are grateful to the Catalina Real-time Transient Survey team for making their photometric database available to the public. We acknowledge with thanks the variable star observations from the AAVSO International Database contributed by observers worldwide and used in this research. We thank an anonymous referee for improving the paper. We thank K. Isogai and

T. Ohshima for helping the compilation of the observation.

References

- Andronov, I. L. 1991, *IBVS*, 3614, 1
 Araujo-Betancor, S., et al. 2005, *A&A*, 430, 629
 Augusteijn, T., & Wisotzki, L. 1997, *A&A*, 324, L57
 Baba, H., Kato, T., Nogami, D., Hirata, R., Matsumoto, K., & Sadakane, K. 2000, *PASJ*, 52, 429
 Bianchini, A., Sabbadin, F., Favero, G. C., & Dalmeri, I. 1986, *A&A*, 160, 367
 Chen, A., O’Donoghue, D., Stobie, R. S., Kilkenny, D., & Warner, B. 2001, *MNRAS*, 325, 89
 Cleveland, W. S. 1979, *J. Amer. Statist. Assoc.*, 74, 829
 de Martino, D., et al. 2005, *A&A*, 437, 935
 Drake, A. J., et al. 2009, *ApJ*, 696, 870
 Evans, P. A., & Hellier, C. 2005, *MNRAS*, 359, 1531
 Fernie, J. D. 1989, *PASP*, 101, 225
 Geßner, H. 1989, *Mitteil. Veränderl. Sterne*, 11, 186
 Hellier, C. 2001, *Cataclysmic Variable Stars: How and why they vary* (Berlin: Springer)
 Hirose, M., & Osaki, Y. 1990, *PASJ*, 42, 135
 Ishioka, R., Kato, T., Matsumoto, K., Uemura, M., Iwamatsu, H., & Stubbings, R. 2001, *IBVS*, 5023
 Ishioka, R., et al. 2002, *PASJ*, 54, 581
 Kato, T., et al. 2014a, *PASJ*, in press (arXiv/1406.6428)
 Kato, T., et al. 2013a, *PASJ*, 65, 23
 Kato, T., et al. 2014b, *PASJ*, 66, 30
 Kato, T., et al. 2009a, *PASJ*, 61, S395
 Kato, T., & Maehara, H. 2013, *PASJ*, 65, 76
 Kato, T., et al. 2010, *PASJ*, 62, 1525
 Kato, T., Monard, B., Hamsch, F.-J., Kiyota, S., & Maehara, H. 2013b, *PASJ*, 65, L11
 Kato, T., & Osaki, Y. 2013, *PASJ*, 65, 115
 Kato, T., et al. 2009b, *PASJ*, 61, 601
 Kato, T., & Uemura, M. 2012, *PASJ*, 64, 122
 Kemp, J., Patterson, J., Thorstensen, J. R., Fried, R. E., Skillman, D. R., & Billings, G. 2002, *PASP*, 114, 623
 Mukadam, A. S., et al. 2010, *ApJ*, 714, 1702
 Neustroev, V., et al. 2012, *Mem. Soc. Astron. Ital.*, 83, 724
 Neustroev, V. V., Tovmassian, G. H., Zharikov, S. V., & Sjöberg, G. 2013, *MNRAS*, 432, 2596
 Nogami, D., Baba, H., Kato, T., & Novák, R. 1998, *PASJ*, 50, 297
 Osaki, Y. 1989, *PASJ*, 41, 1005
 Osaki, Y. 1996, *PASP*, 108, 39
 Osaki, Y., & Kato, T. 2013a, *PASJ*, 65, 50
 Osaki, Y., & Kato, T. 2013b, *PASJ*, 65, 95
 Patterson, J. 1994, *PASP*, 106, 209
 Patterson, J., Augusteijn, T., Harvey, D. A., Skillman, D. R., Abbott, T. M. C., & Thorstensen, J. 1996, *PASP*, 108, 748
 Patterson, J., Schwartz, D. A., Pye, J. P., Blair, W. P., Williams, G. A., & Caillault, J.-P. 1992, *ApJ*, 392, 233
 Patterson, J., & Szkody, P. 1993, *PASP*, 105, 1116
 Schwöpe, A., et al. 2000, *Astron. Nachr.*, 321, 1
 Silvestri, N. M., Szkody, P., Mukadam, A. S., Hermes, J. J., Seibert, M., Schwartz, R. D., & Harpe, E. J. 2012, *AJ*, 144, 84
 Skidmore, W., Mason, E., Howell, S. B., Ciardi, D. R., Littlefair, S., & Dhillon, V. S. 2000, *MNRAS*, 318, 429
 Stellingwerf, R. F. 1978, *ApJ*, 224, 953
 Tappert, C., Augusteijn, T., & Maza, J. 2004, *MNRAS*, 354, 321

recorded in the AAVSO database and we do not consider it convincing. Since this faster fading rate was recorded only for a brief time (less than 1 d), intrinsic erratic variations of the object or systematic difference in the zero-point between different observers may have affected the conclusion in Neustroev et al. (2012).

- Thorstensen, J. R., Patterson, J. O., Shambrook, A., & Thomas, G. 1996, *PASP*, 108, 73
- Tibshirani, R. 1996, *J. R. Statistical Soc. Ser. B*, 58, 267
- Tovmassian, G. H., et al. 1998, *A&A*, 335, 227
- Vogt, N. 1983, *A&A*, 118, 95
- Warner, B. 1995, *Cataclysmic Variable Stars* (Cambridge: Cambridge University Press)
- Warner, B., & Pretorius, M. L. 2008, *MNRAS*, 383, 1469
- Watson, M. G., King, A. R., & Osborne, J. 1985, *MNRAS*, 212, 917
- Woudt, P. A., et al. 2012, *MNRAS*, 427, 1004
- Zharikov, S., Tovmassian, G., Aviles, A., Michel, R., Gonzalez-Buitrago, D., & Garcia-Diaz, M. T. 2013, *A&A*, 549, A77